Specific mitochondrial DNA mutation in mice regulates diabetes and lymphoma development

Osamu Hashizume[a], Akinori Shimizu[a], Mutsumi Yokota[a], Atsuko Sugiyama[a], Kazuto Nakada[a], Hiroyuki Miyoshi[b], Makiko Itami[c], Miki Ohira[d], Hiroki Nagase[e], Keizo Takenaga[f], and Jun-Ichi Hayashi[a,1]

[a]Faculty of Life and Environmental Sciences, University of Tsukuba, 1-1-1 Tennodai, Tsukuba, Ibaraki 305-8572, Japan, [b]Subteam for Manipulation of Cell Fate, RIKEN BioResource Center, Tsukuba, Ibaraki 305-0074, Japan, [c]Department of Pathology, Chiba Cancer Center, 666-2 Nitona-Cho, Chuo-Ku, Chiba 260-8717 Japan, [d]Division of Cancer Genomics, Chiba Cancer Center Research Institute, 666-2 Nitona-Cho, Chuo-Ku, Chiba 260-8717 Japan, [e]Division of Cancer Genetics, Chiba Cancer Center Research Institute, 666-2 Nitona-Cho, Chuo-Ku, Chiba 260-8717 Japan, and [f]Department of Life Science, Shimane University Faculty of Medicine, 89-1 Enya-cho, Izumo, Shimane 693-8501, Japan.

[1]To whom correspondence should be addressed. Email: J.-I.H. (jih45@biol.tsukuba.ac.jp).

ABSTRACT

It has been hypothesized that respiration defects caused by accumulation of pathogenic mitochondrial DNA (mtDNA) mutations and the resultant overproduction of reactive oxygen species (ROS) or lactates are responsible for aging and age-associated disorders, including diabetes and tumor development. However, there is no direct evidence to prove the involvement of mtDNA mutations in these processes, because it is difficult to exclude the possible involvement of nuclear DNA mutations. Our previous studies resolved this issue by using an mtDNA exchange technology and showed that a G13997A mtDNA mutation found in mouse tumor cells induces metastasis via ROS overproduction. Here, using transmitochondrial mice (mito-mice), which we had generated previously by introducing G13997A mtDNA from mouse tumor cells into mouse embryonic stem cells, we provide convincing evidence supporting part of the abovementioned hypothesis by showing that G13997A mtDNA regulates diabetes development, lymphoma formation, and metastasis—but not aging—in this model.

INTRODUCTION

Pathogenic mtDNA mutations that induce significant mitochondrial respiration defects are responsible for mitochondrial diseases (1, 2) and could also be involved in aging and age-associated disorders, including tumor development (1–5). On the other hand, mitochondrial respiration defects caused by nuclear DNA mutations and the resultant enhanced glycolysis under normoxic conditions, i.e., the Warburg effect, are proposed to be involved in tumor development (6–9). Because pathogenic mtDNA mutations also induce mitochondrial

respiration defects and upregulation of aerobic glycolysis, accumulation of these mtDNA mutations with age could also be responsible for tumor development. In addition, it is possible that mtDNA mutations regulate tumor development as a consequence of overproduction of reactive oxygen species (ROS) and the resultant induction of genetic instability (1, 2, 10). In fact, somatic mtDNA mutations are preferentially accumulated in human tumor cells (11–13), and a germline mtDNA mutation (A8344G) in the tRNA^{Lys} gene has been found in lipomas (benign adipose tissue tumors) (14). However, there is as yet no direct evidence for the contribution of mtDNA mutations to aging and tumor development, because of the difficulty of excluding the possible contribution of nuclear DNA mutations, including copy number variants (CNVs), to these processes (2, 15).

Our previous study (16) resolved this issue by using complete mtDNA exchange technology between mouse normal and tumor cells, and we showed that exogenously introduced mtDNA does not affect tumorigenicity. In contrast, our recent study (17) performed exchange of mtDNA between poorly and highly metastatic mouse tumor cells, providing convincing evidence that the somatic mtDNA mutation G13997A in the ND6 gene, which encodes one of the subunits of respiration complex I (NADH dehydrogenase), reversibly controls the development of highly metastatic potential in tumor cells. Moreover, the induction of metastasis is due to overproduction of ROS (17) but not to overproduction of lactates (18). However, these studies have not answered the questions of whether the mutated mtDNA actually controls metastatic phenotypes in living mice and whether it also controls aging and age-associated disorders, including tumor development. Because it is not possible to examine these questions as far as the mutated mtDNA is confined in tumor cells, we performed intercellular transfer of G13997A mtDNA from highly metastatic tumor cells into mouse embryonic stem cells, and generated transmitochondrial mito-mice possessing only G13997A mtDNA (19).

This study used aged inbred C57BL/6J (B6) mice and age-matched mito-mice (named mito-miceND6^M), which carry G13997A mtDNA but share the B6 nuclear background to exclude the possible involvement of nuclear DNA variations in the phenotypes exclusively developed in aged mito-miceND6^M. We examined whether aged mito-miceND6^M with G13997A mtDNA introduced from the highly metastatic tumor cells would be susceptible to aging and to age-associated disorders such as tumor development.

Results

Mitochondrial Disease Phenotypes in Aged Mito-miceND6^M. Using the aged transmitochondrial mito-miceND6^M, we first examined whether aging enhances respiration defects and the phenotypes associated with mitochondrial diseases. Complex I activity in the tissues of aged mito-miceND6^M (18-month-old males) was about 35% to 40% lower than that in age-matched B6 males (Fig. 1*A*). In aged mito-miceND6^M, ROS were overproduced in bone marrow cells but not in splenocytes (Fig. 1*B*). Considering that young mito-miceND6^M (3-month-old males) show a 30% reduction in complex I activity and no ROS overproduction (19), aging enhanced these phenotypes.

Our previous study (19) also showed that young mito-miceND6^M (3-month-old males) have slight lactic acidosis, a common phenotype in humans with mitochondrial diseases (1, 2) and in mito-mice with other pathogenic mtDNA mutations (20–22). Using aged mito-miceND6^M (21-month-old males), this study reexamined blood lactate levels. We also used mito-miceCOI^M, which we had generated previously (21), as positive controls with lactic acidosis due to respiration complex IV defects caused by a pathogenic T6589C mtDNA mutation in the COI gene. Unlike B6 mice, both aged mito-miceND6^M and age-matched

mito-miceCOI[M] (21-month-old males) had slight lactic acidosis in the peripheral blood (Fig. 1*C*). Induction of lactic acidosis, i.e., the Warburg effect, was therefore common to the two mutants (mito-miceND6[M] and mito-miceCOI[M]), irrespective of whether they were young or aged or whether they express respiration defects in complex I or IV activity.

In addition to lactic acidosis, aged patients with mitochondrial diseases sometimes express diabetes, which is one of the age-associated disorders considered to be caused by mtDNA mutations (1, 2). We therefore examined blood glucose and insulin levels. Although we found no significant differences in blood insulin levels between aged mito-miceND6[M] (21-month-old males) and age-matched B6 males (Fig. S1), aged mito-miceND6[M] had higher blood glucose levels after glucose stimulation than did age-matched B6 mice; however, glucose levels in aged mito-miceCOI[M] did not differ from those in age-matched B6 mice (Fig. 1*D*). Therefore, all pathogenic mtDNA mutations, inducing mitochondrial respiration defects, do not necessarily cause mitochondrial diabetes. Because the G13997A mutation, but not the T6589C mutation, induces ROS overproduction (17), the increased glucose levels observed exclusively in aged mito-miceND6[M] might have resulted not from lactate overproduction but from ROS overproduction. This idea was supported by the results of administration of *N*-acetylcysteine (NAC), an antioxidant, to the mito-miceND6[M]: NAC treatment for 1 week suppressed the glucose intolerance (Fig. S2).

Lifespan and Tumor Formation Frequency in Mito-MiceND6[M]. Respiration defects caused by mtDNA mutations and the resultant overproduction of ROS and lactates are also considered to induce aging and age-associated disorders, including tumor formation (1–4, 6–13, 23, 24). We therefore examined this hypothesis by using 35 mito-miceND6[M] males and 35 B6 males. We also examined 18 mito-miceCOI[M] males as

controls expressing lactic acidosis (Fig. 1*C*) to test whether the lactic acidosis common to mito-miceND6^M and mito-miceCOI^M would affect lifespan and tumor formation frequency.

Median survival times of mito-miceND6^M, B6 mice, and mito-miceCOI^M were 24.6, 26.1, and 26.6 months, respectively. Although mito-miceND6^M had slightly shorter survival times than B6 mice, the difference was not significant (Fig. 2*A*). No leukemic cells were present in the peripheral blood throughout the lifespans of B6 and mutant mice. However, gross necropsy of all dead or euthanized moribund mice showed that 16 of 35 mito-miceND6^M (45.7%) had macroscopic tumor-like abnormalities, including enlarged spleen and liver and lymph node tumors (Table 1 and Fig. 3*A*); similar abnormalities were observed in only three of 35 B6 mice (8.6%) and one of 18 mito-miceCOI^M (5.6%). The median survival times of mice without tumor-like abnormalities were 25.3 (mito-miceND6^M), 26.0 (B6 mice), and 26.6 months (mito-miceCOI^M); these differences were not significant (Fig. 2*B*). The slightly shorter median survival times of mito-miceND6^M compared with those of B6 mice (Fig. 2*A*) were therefore at least partly due to the higher frequency of abnormal-tissue formation in aged mito-miceND6^M than in age-matched B6 mice (Table 1).

Histological analyses of abnormal tissues revealed that all were hematopoietic neoplasms and were positive for the pan-leukocyte marker CD45 (Table 1 and Fig. 3*B*). As no leukemic cells were observed in the peripheral blood (Fig. 3*A*), these hematological neoplasms may have consisted of lymphoma cells. Most tumors were of B-cell origin, expressing the B-cell marker B220 (CD45R) (Fig. 3*B*); they were either follicular lymphoma or diffuse large B-cell lymphoma arising in the spleen, liver, or lung (Table 1). One aged mito-miceND6^M male and one aged B6 male developed T-cell lymphoma, staining positive for the T-cell marker CD3 (Table 1). These data indicated that mito-

miceND6^M were 750% more prone to lymphoma development than B6 mice in a B cell–specific manner, providing unambiguous evidence supporting the hypothesis that mitochondrial respiration defects are responsible for tumor formation. However, respiration defects and the resultant lactic acidosis alone could not have been responsible for the frequent B-cell lymphoma formation in the mito-miceND6^M, because aged mito-miceCOI^M, which also showed respiration defects and resultant lactic acidosis (Fig. 1C), did not have high frequencies of lymphoma formation (Table 1). It is therefore likely that the ROS overproduction in the bone marrow of mito-miceND6^M (Fig. 1B) is crucial for B-cell lymphoma formation. Analysis of the CNVs showed partial gains of chromosomes 3 and 11 in the spleen with B-cell lymphoma from a mito-mouseND6^M (Fig. S3), suggesting that G13997A mtDNA and the resultant ROS overproduction and chromosome aberration are involved in B-cell lymphoma development.

Metastatic Potential in Mito-miceND6^M. Mito-miceND6^M did not form tumors other than lymphomas during their lifespans (Table 1). Thus, the tumor-inducing effect of G13997A mtDNA might be restricted to lymphoma formation, and it might therefore be difficult to examine the effects of G13997 mtDNA on metastatic potential in mito-miceND6^M. We examined these possibilities by isolating mouse embryonic fibroblasts (MEFs) and testing whether G13997A mtDNA affected their tumor-related phenotypes, such as immortalization of MEFs to lose their finite lifespan, transformation of immortalized MEFs to acquire tumorigenicity, or malignant progression of the transformed MEFs to express metastasis.

We obtained three MEF lines (MEFB6-I, -II, -III) from three B6 embryos and four lines (MEFND6^M-I, -II, -III, -IV) from four mito-miceND6^M embryos (Table S1). By culturing these seven MEF lines using the 3T3 protocol (25, 26; see Methods), we isolated six

immortalized 3T3 lines (3T3B6-I, -II, -III; 3T3ND6^M-I, -II, -III); we failed to obtain one

3T3 line from an MEF line (MEFND6^M-IV) with G13997A mtDNA (Table S1). The

average numbers of cell divisions for the MEF lines to lose their finite lifespan were 7.9 for

MEFB6 and 11.0 for MEFND6^M (Fig. 4A), suggesting that at least three additional cell

divisions were required for immortality in MEFND6^M with G13997A mtDNA. Therefore,

G13997A mtDNA does not enhance, but instead slightly suppresses, immortalization in

MEFs.

Next, we examined the frequency of spontaneous transformation of immortalized 3T3 lines

into tumor cells expressing tumorigenicity. After we had established six immortal 3T3 lines,

we cultured them for 1 month to obtain sufficient numbers of cells for inoculation to test

their tumorigenicity. After inoculating the cells subcutaneously into the backs of B6 mice,

we observed growing tumor masses only from the inoculation of two 3T3 lines, 3T3B6-III

and 3T3ND6^M-I, carrying B6 mtDNA and G13997A mtDNA, respectively; the other four

3T3 lines did not form tumor masses (Fig. 4B). These four non-transformed 3T3 lines were

cultured for 3 months more to allow spontaneous transformation. They were then

inoculated again subcutaneously into the backs of B6 mice. Two 3T3 lines, 3T3B6-II and

3T3ND6^M-III, formed tumors (Fig. 4B), probably because of their spontaneous

transformation to acquire tumorigenicity during prolonged cultivation. These observations

suggest that some of the cells in the populations of the four immortal 3T3 lines had already

been transformed spontaneously, and that G13997A mtDNA did not necessarily enhance

the transformation frequency of immortalized 3T3 cells to acquire tumorigenicity.

To purify the transformed cells in the population of the four 3T3 line, tumor masses formed

from the inoculations under the skin of B6 mice (Fig. 4B) were cut into small pieces and

placed back into culture medium. Growing cells in culture were obtained from all tumor

masses. These cells were then inoculated again subcutaneously into the backs of B6 mice. All of them rapidly formed tumor masses (Fig. 4C), suggesting that they were fibrosarcoma lines expressing tumorigenicity. The lines were named FSB6-II, FSB6-III, FSND6^M-I, and FSND6^M-III (Table S1). FSB6-II and FSB6-III were confirmed to possess wild-type (B6) mtDNA, and FSND6^M-I and FSND6^M-III possessed G13997A mtDNA (Fig. 4D).

We then examined the metastatic potential of the fibrosarcoma lines by inoculating them intravenously into B6 mice and counting nodule numbers in the lung. This malignant tumor phenotype was exclusively enhanced in the fibrosarcoma cell lines FSND6^M-I and -III (Fig. 4E), which carried G13997A mtDNA (Fig. 4D), even though their primary tumor growth was slower than that of FSB6-II and -III (Fig. 4C), which had B6 mtDNA (Fig. 4D). Therefore, G13997A mtDNA did not enhance immortalization and transformation of MEFs, but it enhanced the malignant progression of spontaneously-transformed MEFs to acquire high metastatic potential.

Discussion

Here, we used aged mito-miceND6^M with pathogenic G13997A mtDNA to examine conventional mitochondrial theory (1–5) proposing that respiration defects caused by pathogenic mtDNA mutations and the resultant ROS or lactate overproduction are responsible for aging and age-associated disorders. As controls we used age-matched B6 mice with normal mtDNA and mito-miceCOI^M mice with pathogenic T6589C mtDNA (21), which induces respiration defects and the resultant lactate overproduction but not ROS overproduction (17). All of the mice used in this study shared the B6 nuclear DNA background, thus excluding the possible involvement of nuclear genetic variations in the

phenotypes exclusively developed in mito-miceND6^M. The results showed that neither

G13997A mtDNA nor T6589C mtDNA enhanced aging, but that G13997A mtDNA

induced B-lymphoma formation and glucose intolerance, whereas T6589C mtDNA did not.

Therefore, this study provides convincing evidence that some pathogenic mtDNA

mutations, such as the G13997A mutation, regulate age-associated disorders, including B-

lymphoma development and diabetes, in living mice. Moreover, G13997A mtDNA

appeared to play various roles in the multiple steps required for MEF transformation. For

example, G13997A mtDNA slightly suppressed immortalization of MEFs to loose their

finite lifespan (Fig. 4*A*), and it did not induce transformation of immortalized MEFs to

acquire tumorigenicity (Fig. 4*B*). However, it did induce malignant progression of the

transformed MEFs to express high metastatic potential (Fig. 4*E*). These results are

consistent with our previous observations (17): using an *in vitro* culture system we

previously showed that the G13997A mutation induced malignant progression of lung

carcinoma cells to acquire high metastatic potential, but it did not induce transformation of

immortalized NIH3T3 cells to acquire tumorigenicity (17). Therefore, our finding here that

the mutation induced frequent B-lymphoma development in mito-miceND6^M (Table 1) was

unexpected.

The question that then arises is why were there only hematological malignancies (Table 1)

despite the fact that respiration defects affected all of the tissues examined (Fig. 1*A*). One

answer to this tissue-specific tumor development is that the nuclear genetic background of

the B6 mice used in this study made them prone to B-lymphoma formation but not to other

tumors during their lifespans (Table 1). This idea can be examined by generating mito-

miceND6^M carrying G13997A mtDNA but in a nuclear genetic background derived from

another wild-type mouse strain that preferentially develops tumors other than B-lymphoma.

It has been proposed that nuclear genetic variations among wild-type mouse strains affect

the tumor formation spectrum (27-30), particularly when genetic manipulations are performed to induce tumor development (29, 30). Thus the generation of new mito-miceND6^M would be effective for examining the issue of whether G13997A mtDNA enhances the development of different tumors in different nuclear genetic backgrounds, or whether it specifically enhances B-lymphoma development irrespective of whether the nuclear genetic background is derived from B6 or not.

Another question is the nature of the mechanism of B-lymphoma development in mito-miceND6^M. Analysis of CNVs showed partial gains of chromosomes 3 and 11 in a spleen with B-lymphoma from a mito-mouseND6^M (Fig. S3). Thus, one possible mechanism could be chromosomal instability caused by G13997A mtDNA–mediated overproduction of ROS. It has been proposed that oxidative stress induces various types of cellular damage, leading to chromosome instability that can result in tumor development (10). Moreover, B-lymphomas can be frequently induced as a consequence of chromosome translocation (31). Precise chromosome analysis may therefore reveal the mechanism of frequent B-lymphoma formation in mito-miceND6^M.

With respect to the aging of mito-miceND6^M, the G13997A mutation does not solely enhance aging or regulate premature aging phenotypes, which have been reported in mtDNA mutator mice possessing nuclear-coded mtDNA polymerase with a defective proofreading function and expressing the resultant mitochondrial respiration defects but not ROS overproduction (32-34). Absence of the premature aging phenotypes in mito-miceND6^M is not unexpected, because there is no evidence that patients with mitochondrial diseases due to pathogenic mtDNA mutations develop generalized premature aging. Therefore, the introduction of different nuclear genetic backgrounds or nuclear DNA

variations into mito-miceND6^M may be required to trigger the onset of their premature aging phenotypes.

Our results also suggested that the glucose intolerance observed exclusively in aged mito-miceND6^M (Fig. 1*D*) resulted from ROS overproduction. This idea was confirmed by the observation that NAC administration suppressed glucose intolerance (Fig. S2). Continuous NAC administration could therefore be an effective therapy for improving ROS-mediated diabetic phenotypes. Because it has been proposed that ROS negatively controls insulin secretion from pancreatic β cells or glucose incorporation into insulin-targeted organs in humans (35), mito-miceND6^M would be effective models for precise investigation of the mechanisms of ROS-mediated diabetes. On the other hand, a reduction in ATP content caused by mitochondrial respiration defects in pancreatic β cells has also been proposed to suppress their insulin secretion and could thus be responsible for inducing mitochondrial diabetes (36). In fact, patients with mitochondrial diseases who carry an A3243G mtDNA mutation in the mitochondrial tRNA$^{Leu(UUR)}$ gene frequently express diabetic phenotypes (1, 35, 37). However, other pathogenic mtDNA mutations are not necessarily correlated with these phenotypes (37). Our mito-miceCOI^M did not show glucose intolerance (Fig. 1*D*), indicating that respiration defects do not always induce diabetic phenotypes. Other mito-mice carrying a pathogenic mutation in the mitochondrial tRNA$^{Leu(UUR)}$ gene will therefore have to be generated to resolve this controversy over the pathogenesis of mitochondrial diabetes.

Materials and Methods

Mice. Inbred B6 mice generated by sibling mating more than 40 times were obtained from CLEA Japan. Mito-miceND6^M (19) and mito-miceCOI^M (21) were generated in our

previous works. We maintained B6 mice, mito-miceND6^M, and mito-miceCOI^M sharing a common nuclear DNA background by repeated backcrossing of their females with B6 males. Animal experiments were performed in accordance with protocols approved by the Experimental Animal Committee of the University of Tsukuba, Japan.

Cell Lines and Cell Culture. The mouse cell lines obtained were grown in DMEM (Sigma) containing 10% (vol/vol) FCS, uridine (50 ng/ml), and pyruvate (0.1 mg/ml).

Biochemical Measurement of Respiratory Enzyme Activity. Mitochondrial respiratory complex I (NADH dehydrogenase), complex II (succinate dehydrogenase), and complex III (cytochrome *c* reductase) are components of the electron-transport chain and are located in the mitochondrial inner membrane. The activity of these enzymes was assayed as described previously (11). Briefly, to estimate complex I + III activity, NADH and cytochrome *c* (oxidized form) were used as substrates and the reduction of cytochrome *c* was monitored by measuring absorbance at a wavelength of 550 nm. To estimate complex II + III activity, sodium succinate and cytochrome *c* (oxidized form) were used as substrates, and the reduction of cytochrome *c* was monitored as described above.

Measurement of ROS Production in Mitochondria. ROS generation was detected with the mitochondrial superoxide indicator MitoSOX-Red (Invitrogen). Cells were incubated with 1 mM MitoSOX-Red for 15 min at 37 ºC in phosphate-buffered saline (PBS), washed twice with PBS, and then immediately analyzed with a FACScan flow cytometer (Becton Dickinson).

Lactate and Glucose Measurement. To determine fasting blood lactate and glucose concentrations, blood was collected from the tail veins of mice after overnight starvation. After oral administration of glucose (1.5 g/kg body weight), blood was again collected, and lactate and glucose concentrations were measured with an automatic blood lactate test meter (Lactate Pro, Arkray) and glucose test meter (Dexter ZII, Bayer), respectively.

Blood Insulin Measurement. Peripheral bloods were collected from tail veins. After centrifugation of the blood at 1000g for 15 min at 4 ºC, the plasma fraction collected from the supernatant was used to estimate blood insulin levels with a mouse insulin ELISA kit (Shibayagi).

Histological Analyses. Formalin-fixed, paraffin-embedded serial sections were used for histological analyses. Hematoxylin and eosin–stained sections were used for histopathological analysis to identify tumor tissues. The immunohistochemical analysis was performed with antibody to CD45 (BD Biosciences) to determine whether the tumor tissues originated from leukocytes, and subsequently with antibodies to B220 (BD Biosciences) and CD3 (Santa Cruz) to determine whether the tumor tissues were of B-cell or T-cell origin, respectively.

Analysis of CNVs. Copy number variations in nuclear DNA were examined by array CGH (comparative genomic hybridization) using a 4×44k whole-genome array (Agilent Technologies G4426B#15028). DNA (1 μg) derived from each male mouse spleen was used. A dye-swap experiment was conducted to confirm the results. The protocol for DNA digestion, labeling, purification, and hybridization to the arrays followed the manufacturers' instructions (Agilent Technologies).

Isolation of Immortal 3T3 Cells from MEFs. MEFs in a 6-cm culture dish at a density

of 3×10^5 cells per dish were cultured by using the 3T3 protocol reported previously (25, 26).

Briefly, 3 days after the cells had been plated at 3×10^5 cells per dish, we trypsinized them,

counted the total cell numbers, and then replated 3×10^5 cells into 6-cm dishes. These

processes were repeated until immortalized cells appeared.

Genotyping of mtDNAs. Total cellular DNA (0.2 mg) extracted from cultured cells was

used as a template. To detect the G13997A mutation, a 147-bp fragment containing the

13997 site was amplified by using PCR. The nucleotide sequences from nucleotide

positions 13963 to 13996 (5′-CCCACTAACAATTAAACCTAAACCTCCATActTA-3′;

small letters indicate the mismatch site) and nucleotide positions 14109 to 14076 (5′-

TTCATGTCATTGGTCGCAGTTGAATGCTGTGTAG-3′) were used as oligonucleotide

primers. Combination of the PCR-generated mutation with the G13997A mutation created a

restriction site for *Afl* II and generated 114-bp and 33-bp fragments on *Afl* II digestion.

Restriction fragments were separated by electrophoresis on 3% agarose gels containing

ethidium bromide (0.1 mg/ml).

Assays of Metastatic Potential and Tumorigenicity. To test for experimental

metastatic potential, cells (5×10^5/100 μl PBS) were injected into the tail vein of 6-week-old

male B6 mice (CLEA Japan). The mice were euthanized 23 days later, and their lungs were

removed. The lungs were fixed in Bouin's solution and parietal nodules were counted. To

assess tumorigenicity, growing cells (5×10^6 cells) suspended in 100 μl PBS were injected

subcutaneously into the backs of 5 week-old male B6 mice. Tumor growth was monitored

assuming spherical growth. When a tumor mass was detectable visually, its maximum (a)

and minimum (b) diameters and height (h) were recorded twice a week. The volume of

each tumor (V) was calculated according to the formula $V = \pi abh/6$.

Statistical Analysis. We analyzed data with the (unpaired or paired) Student's *t*-test.

Kaplan–Meier curves were assessed with the log-rank test. Values with $P < 0.05$ were

considered significant.

REFERENCES

1. Wallace DC (1999) Mitochondrial diseases in man and mouse. *Science* 283:1482–1488.

2. Taylor RW, Turnbull DM (2005) Mitochondrial DNA mutations in human disease. *Nat Rev Genet* 6:389–402.

3. Jacobs HT (2003) The mitochondrial theory of aging: dead or alive? *Aging Cell* 2:11–17.

4 Khrapko K, Vija J (2008) Mitochondrial DNA mutations and aging: devils in the details? *Trends Genet* 25:91–98.

5. Loeb LA, Wallace DC, Martin GM (2005) The mitochondrial theory of aging and its relationship to reactive oxygen species damage and somatic mtDNA mutations. *Proc Natl Acad Sci USA* 102:18769–18770.

6. Baysal BE, et al. (2000) Mutations in SDHD, a mitochondrial complex II gene, in hereditary paraganglioma. *Science* 287:848–851.

7. Niemann S, Muller U (2000) Mutations in SDHC cause autosomal dominant paraganglioma, type 3. *Nat Genet* 26:268–270.

8. Gottlieb E, Tomlinson IP (2005) Mitochondrial tumor suppressors: a genetic and biochemical update. *Nat Rev Cancer* 5:857–866.

9. Koppenol WH, Bounds PL, Dang CV (2011) Otto Warburg's contributions to current concepts of cancer metabolism. *Nat Rev Cancer* 11:325–337.

10. Klaunig JE, Kamendulis LM, Hocevar BA (2010) Oxidative stress and oxidative damage in carcinogenesis. *Toxicologic Pathol* 38:96–109.

11. Polyak K, et al. (1998) Somatic mutations of the mitochondrial genome in human colorectal tumors. *Nat Genet* 20:291–293.

12. Fliss MS, et al. (2000) Facile detection of mitochondrial DNA mutations in tumors and bodily fluids. *Science* 287:2017–2019.

13. Yiping H, et al. (2010) Heteroplasmic mitochondrial DNA mutations in normal and tumor cells. *Nature* 464:610–614.

14. Larsson NG, Tulinius MH, Oldfas A (1995) Pathogenetic aspects of the A8344G mutation of mitochondrial DNA associated with MERRF syndrome and multiple symmetric lipomas. *Muscle Nerve* 3:S102–S106.

15. Augenlicht LH, Heerdt B (2001) Mitochondria: integrators in tumorigenesis? *Nat Genet* 28:104–105.

16. Akimoto M, et al. (2005) Nuclear DNA but not mtDNA controls tumor phenotypes in mouse cells. *Biochem Biophys Res Commun* 327:1028–1035.

17. Ishikawa K, et al. (2008) ROS-generating mitochondrial DNA mutations can regulate tumor cell metastasis. *Science* 320:661–664.

18. Ishikawa K, et al. (2008) Enhanced glycolysis induced by mtDNA mutations does not regulate metastasis. *FEBS Lett* 582:3525–3530.

19. Yokota M, et al. (2010) Generation of trans-mitochondrial mito-mice by the introduction of a pathogenic G13997A mtDNA from highly metastatic lung carcinoma cells. *FEBS Lett* 584:3943–3948.

20. Inoue K, et al. (2000) Generation of mice with mitochondrial dysfunction by introducing mouse mtDNA carrying a deletion into zygotes. *Nat Genet* 26:176–181.

21. Kasahara A, et al. (2006) Generation of trans-mitochondrial mice carrying homoplasmic mtDNAs with a missense mutation in a structural gene using ES cells. *Hum Mol Genet* 15:871–881.

22. Nakada K, et al. (2004) Accumulation of pathogenic DeltamtDNA induced deafness but not diabetic phenotypes in mito-mice. *Biochem Biophys Res Commun* 323:0175–184.

23. Shidara Y, et al. (2005) Positive contribution of pathogenic mutations in the mitochondrial genome to the promotion of cancer by prevention from apoptosis. *Cancer Res* 65:1655–1663.

24. Petros JA, et al. (2005) mtDNA mutations increase tumorigenicity in prostate cancer. *Proc Natl Acad Sci USA* 102:719–724.

25. Todaro GJ, Green H (1963) Quantitative studies of the growth of mouse embryo cells in culture and their development into established lines. *J Cell Biol* 17:299–313.

26. Sun H, Taneja R (2007) Analysis of transformation and tumorigenicity using mouse embryonic fibroblast cells. *Methods Mol Biol* 383:303–310.

27. Krupke DM, Begley DA, Sundberg JP, Bult CJ, Eppig JT (2008) The Mouse Tumor Biology database. *Nat Rev Cancer* 8:459-465.

28. Balmain A, Nagase H (1998) Cancer resistance genes in mice: models for the study of tumour modifiers. *Trends Genet* 14:139-144.

29. Harvey M, McArthur MJ, Montgomery CA Jr, Bradley A, Donehower LA. (1993) Genetic background alters the spectrum of tumors that develop in p53-deficient mice. *FASEB J* 7:938-943.

30. Freeman D, et al. (2006) Genetic background controls tumor development in PTEN-deficient mice. *Cancer Res* 66:6492-6496.

31. Kuppers R (2005) Mechanisms of B-cell lymphoma pathogenesis. *Nat Rev Cancer* 5:251–262.

32. Trifunovic A, et al. (2004) Premature ageing in mice expressing defective mitochondrial DNA polymerase. *Nature* 429:417–423.

33. Kujoth GC, et al. (2005) Mitochondrial DNA mutations, oxidative stress, and apoptosis in mammalian aging. *Science* 309:481–484.

34. Trifunovic A, et al. (2005) Somatic mtDNA mutations cause aging phenotypes without affecting reactive oxygen species production. *Pros Natl Acad Sci USA* 102:17993–17998.

35. Evans JL, Goldfine ID, Maddux BA, Grodsky GM. (2003) Perspectives in diabetes: are oxidative stress-activated signalling pathways mediators of insulin resistance and beta-cell dysfunction? *Diabetes* 52:1–8.

36. Maechier P, Wollheim CB (2001) Mitochondrial function in normal and diabetic β-cells. *Nature* 414:807–812.

37. Maassen JA, et al. (2004) Mitochondrial diabetes: Molecular mechanisms and clinical presentation. *Diabetes* 53:S103–S109.

FIGURE LEGENDS

Fig. 1. Examination of the phenotypes associated with mitochondrial diseases in aged mito-miceND6^M.

(*A*) Biochemical analysis of mitochondrial respiratory complex activity in the brain, heart, and skeletal muscles. Respiratory complex I (NADH dehydrogenase), complex II (succinate dehydrogenase), and complex III (cytochrome *c* reductase) are components of the electron-transport chain located in the mitochondrial inner membrane. Because the activity of complexes II + III is normal in the tissues of mito-miceND6^M, the reduced activity of complexes I + III observed in mito-miceND6^M should represent complex I defects. Data are represented as mean values with SD (n = 3). *P < 0.05 compared with control B6 mice. (*B*) Estimation of mitochondrial superoxide (i.e., reactive oxygen species, ROS) levels in bone marrow cells and splenocytes after treatment with MitoSOX-Red (Invitrogen). Relative mitochondrial superoxide levels were expressed as mean fluorescence intensity. Data are represented as mean values with SD (n = 3). *P < 0.05 compared with control B6 mice. (*C*) Estimation of blood lactate levels in aged mito-miceND6^M, age-matched B6 mice, and age-matched mito-miceCOI^M before and after glucose administration. Data are represented as mean values with SD (n = 5). *P < 0.05 compared with control B6 mice. (*D*) Estimation of blood glucose levels in aged mito-miceND6^M, age-matched B6 mice, and age-matched mito-miceCOI^M before and after glucose administration. Data are represented as mean values with SD (n = 5). *P < 0.05 compared with control B6 mice.

Fig. 2. Kaplan–Meier survival curves of mito-miceND6^M.

(*A*) Comparison of lifespan of mice. Median survival times of mito-miceND6^M (n = 35), B6 mice (n = 35), and mito-miceCOI^M (n = 18) were 24.6, 26.1, and 26.6 months, respectively. Survival curves did not differ significantly. (*B*) Comparison of lifespans of mice that died in the absence of detectable B-cell lymphoma. Median survival times of mito-miceND6^M (n = 19), B6 mice (n = 32), and mito-miceCOI^M (n

= 17) were 25.3, 26.0, and 26.6 months, respectively. Survival curves did not differ significantly.

Fig. 3. B-cell lymphoma formation in the tissues of aged mito-miceND6^M.
(*A*) Gross necropsy of euthanized moribund mice, smear samples of peripheral blood stained by Giemsa, and tissues. Left and right panels represent a euthanized moribund B6 mouse without tumors (B6-3) and a euthanized moribund mito-mouseND6^M with tumors (ND6^M -6), respectively. Scale bars, 1 cm. Giemsa-stained preparations show the absence of leukemic cells in the peripheral blood of both B6-3 and ND6^M-6. Scale bars, 50 μm. (*B*) Histological analyses of serial sections of the tissues to identify B-cell lymphoma. HE, hematoxylin and eosin staining to show tumor formation; CD45, immunohistochemistry using antibody to CD45 to detect leukocytes; B220, immunohistochemistry using antibody to B220 to detect B cells; CD3, immunohistochemistry using antibody to CD3 to detect T cells. Whereas the tissues of B6-3 have a normal structure (left panels), those of ND6^M-6 show abnormal growth of B-lymphoma cells, because they were stained positively with CD45 and B220, but not with CD3 (right panels). The spleen was the primary B-lymphoma site, whereas the liver and lung were secondarily involved through hematogenous metastasis: most of the splenic parenchyma was completely replaced by lymphoma cells, whereas there were multiple small foci of perivascular lymphoma cell infiltration in the liver and lung. Scale bars, 200 μm.

Fig. 4. Characterization of mouse embryonic fibroblasts (MEFs) and MEF-derived cell lines isolated from mito-miceND6^M.
(*A*) Numbers of cell divisions of MEF lines required for immortalization; Av., average number of cell divisions. Data are represented as mean values with SD (*n* = 3). *$P < 0.05$ compared with control B6 mice. (*B*) Transformation frequencies of immortalized MEF (3T3) lines to express tumorigenicity. (*C*) Tumor growth of the transformed 3T3 (fibrosarcoma) lines isolated from tumor masses formed (see Fig.

4*B*). Data are represented as mean values with SD (*n* = 3). (*D*) Identification of mtDNA genotypes of transformed 3T3 (fibrosarcoma) lines. The G13997A mtDNA in FSND6^M-I and -III produced 114- and 33-bp fragments owing to the gain of an *Afl* II site by the G13997A substitution in the *ND6* gene, whereas B6 mtDNA without the mutation in FSB6-II and -III produced uncut 147-bp fragments. (*E*) Metastatic potentials of the transformed 3T3 lines (i.e., fibrosarcoma lines). Data are represented as mean values with SD (*n* = 3). *P < 0.05 compared with two B6 fibrosarcoma lines.
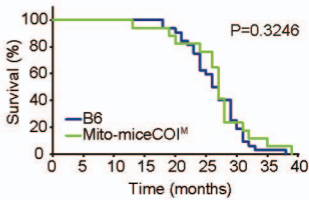
Fig.1

Fig. 2

Fig. 3

A

B6 - 3

ND6^M - 6

Spleen Liver Lung

Spleen Liver Lung

B

B6 - 3

ND6^M - 6

Spleen Liver Lung

Spleen Liver Lung

HE

CD45

B220

CD3
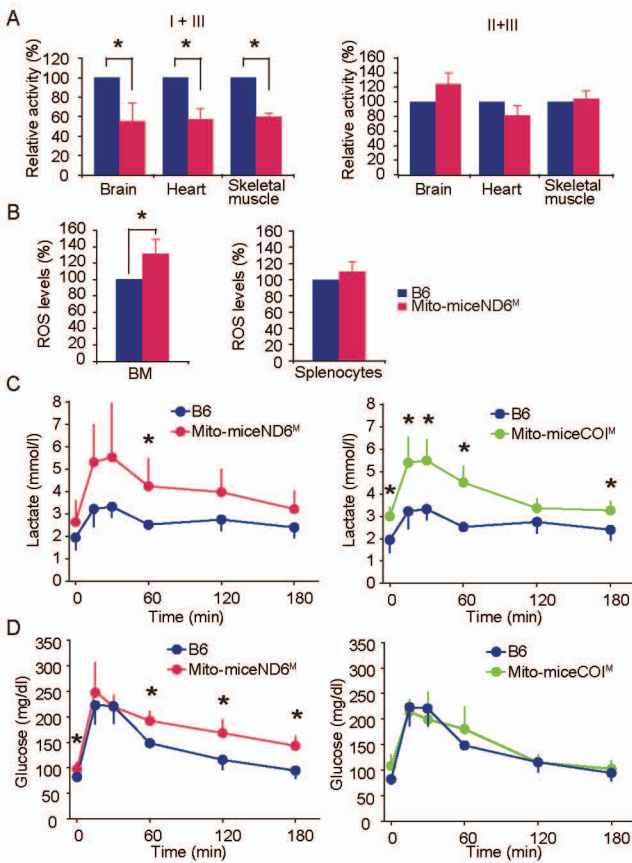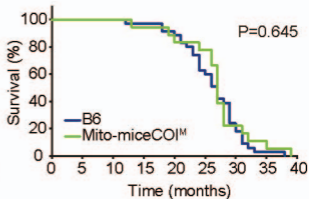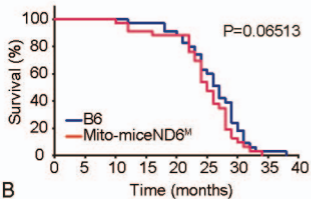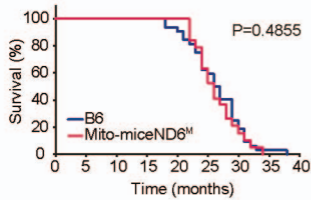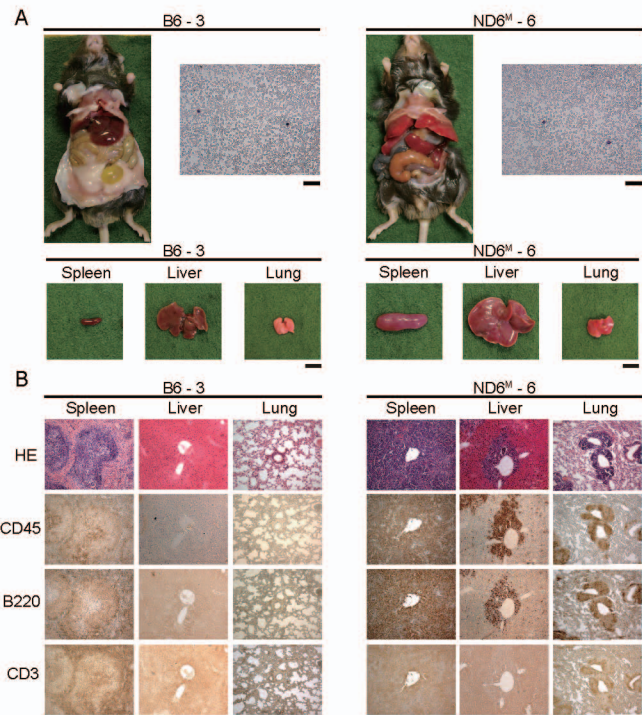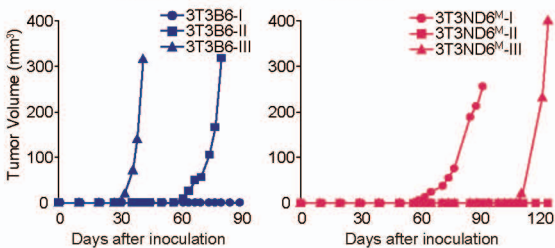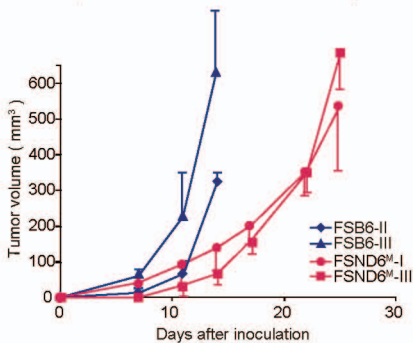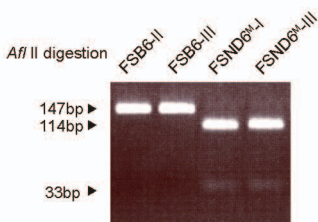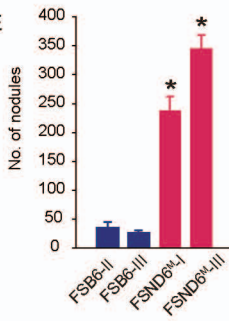
Fig. 4
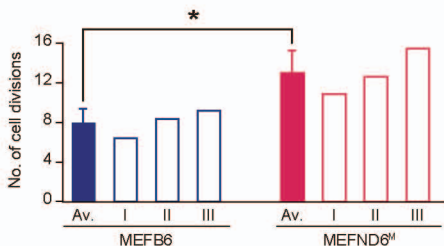
Table 1. Frequencies of lymphoma in dead or moribund mice

Mouse strain	No. of dead mice	No. of dead mice with tumors (individual code*)	Lifespan (months)	Tissue with tumor				Histological analyses†				Cell lineage	Cell type	
				Spleen	Liver	Lung	Lymph node	HE	CD45	B220	CD3		FL	DLBCL
Mito-mice ND6^M	35	16												
		(ND6^M – 31)	29		+		+	Lymphoma	+	+	–	B cell	–	+
		(ND6^M – 29)	28	+				Lymphoma	+	+	–	B cell	–	+
		(ND6^M – 28)	28		+			Lymphoma	+	+	–	B cell	–	+
		(ND6^M – 27)	28	+	+			Lymphoma	+	+	–	B cell	+	–
		(ND6^M – 23)	26	+	+			Lymphoma	+	+	–	B cell	–	+
		(ND6^M – 20)	25		+			Lymphoma	+	+	–	B cell	–	+
		(ND6^M – 18)	24	+			+	Lymphoma	+	+	–	B cell	+	–
		(ND6^M – 13)	23	+			+	Lymphoma	+	–	+	T cell	–	–
		(ND6^M – 11)	22	+	+			Lymphoma	+	+	–	B cell	–	+
		(ND6^M – 7)	19	+				Lymphoma	+	+	–	B cell	–	+
		(ND6^M – 6)	18	+	+	+		Lymphoma	+	+	–	B cell	–	+
		(ND6^M – 5)	18		+			Lymphoma	+	+	–	B cell	–	+
		(ND6^M – 4)	16	+	+	+		Lymphoma	+	+	–	B cell	+	–
		(ND6^M – 3)	12	+				Lymphoma	+	+	–	B cell	–	+
		(ND6^M – 2)	12	+	+			Lymphoma	+	+	–	B cell	–	+
		(ND6^M – 1)	10	+	+			Lymphoma	+	+	–	B cell	+	–
B6	35	3												
		(B6 – 34)	33		+			Lymphoma	+	+	–	B cell	–	+
		(B6 – 14)	25				+	Lymphoma	+	+	–	B cell	–	+
		(B6 – 1)	12		+		+	Lymphoma	+	–	+	T cell	–	–
Mito-mice COI^M	18	1												
		(COI^M – 11)	27				+	Lymphoma	+	+	–	B cell	–	+

DLBCL, diffuse large B-cell lymphoma; FL, follicular lymphoma

* Individual codes were allocated in order of death.

† In most cases, the spleen was the primary B-lymphoma site and the liver and lung were involved secondarily by hematogeneous metastasis (spread), because most of the splenic parenchyma was completely replaced by lymphoma cells, whereas there were multiple small foci of perivascular lymphoma cell infiltration in the liver and lung (see Fig. 3B). In some cases where tumors were present only in the liver or lung, they were not hepatomas or lung carcinomas, but instead were lymphomas that had spread from the spleen or from lymph nodes near the organs, because all stained positively for CD45 and B220 or CD3.